

NOISE DUE TO UNSTEADY FLOW PAST TRAILING EDGES (ECCOMAS CFD 2006)

Richard D. Sandberg*, Neil D. Sandham

University of Southampton, Aerodynamics and Flight Mechanics Research Group,
School of Engineering Sciences, Southampton, SO17 1BJ, United Kingdom

*e-mail: sandberg@soton.ac.uk

web page: <http://www.afm.ses.soton.ac.uk>

Key words: CFD, DNS, aeroacoustic, trailing edge noise

Abstract. *This paper presents two-dimensional direct numerical simulations (DNS) of noise generated at trailing edges (TE) with zero thickness. The simulations are conducted specifying either no-slip or slip walls in order to investigate viscous effects. In both cases, small amplitude disturbances are introduced close to the inflow boundary that serve as pressure disturbances at the TE. DNS data reveals that the unsteady Kutta condition is not satisfied, irrespective of the wall boundary condition. However, it appears that the validity of the unsteady Kutta condition is not essential for making an accurate prediction of the far field noise. The far field pressure is predicted as a function of the surface pressure difference using a 2-D modification of Amiet's classical theory, and compared with the far field pressure computed directly. Directivity plots provide evidence that the presence of boundary layers and noise generated by an unsteady wake in the no-slip cases lead to smearing of individual lobes, and that the downstream pointing lobes in no-slip wall cases are probably due to nonlinear noise generation in the wake. The simulations are conducted using a high-order accurate numerical method which is free of upwinding, artificial dissipation or any form of explicit filtering, and employs a novel boundary treatment.*

1 INTRODUCTION

Noise generated by unsteady flow over trailing edges contributes significantly to airframe noise, fan noise and other sources of sound. Therefore, a detailed understanding of the underlying physical mechanisms in the generation of trailing-edge noise would be beneficial for the design of quieter aircraft and propulsion systems. A theoretical method for calculating the far field noise due to turbulent flow past a trailing edge (TE) was derived in a classical paper by Amiet¹. A closed-form result of the far-field pressure spectrum can be obtained as a function of the convecting incident pressure spectrum upstream of the TE.

The recent dramatic growth in computing power has made direct numerical simulations (DNS) of aerodynamically-generated sound increasingly feasible. Solving the full unsteady

Navier–Stokes equations, both the far field sound and the near field hydrodynamics can be obtained. Thus, DNS can provide an insight into the physical mechanisms of sound generation and potentially help to validate acoustic theories. The aim of the present research is to use DNS data to validate Amiet’s theory. In a previous study², it was demonstrated that the surface pressure jump transfer function performs well for various Mach numbers and reduced frequencies. Here, the focus lies on the radiation of the surface pressure difference to the far field. To that end, an infinitely thin plate is considered with either slip-walls or laminar boundary layers on each side in order to assess the importance of viscous effects. In both cases, small amplitude disturbances are introduced close to the inflow boundary that serve as pressure disturbances at the TE.

To allow for parametric studies, DNS are conducted in two dimensions. Amiet’s classical theory considers three-dimensional sound radiation, hence a modification of Amiet’s theory accounting for two-dimensional sound radiation is derived. The result of the strictly 2-D theory is presented and comparisons between theoretical results and DNS data are made. For the present investigation, a high-order accurate numerical method is chosen which is free of upwinding, artificial dissipation or any form of explicit filtering, as described later. A novel boundary treatment^{3,4} which was developed specifically for, but is not restricted to, the current research is employed.

2 GOVERNING EQUATIONS

2.1 Theoretical Approach

In the present investigation, two-dimensional laminar flows with single-frequency disturbances are investigated. Therefore, a modification of Amiet’s theory accounting for two-dimensional sound radiation of single-frequency disturbances was derived². Here, only the relevant results of the derivation are presented. The two-dimensional theory is applicable in the coordinate system $\underline{x} = [x_1 x_2]^T$, where x_1 and x_2 are the streamwise and the wall normal directions, nondimensionalized with the semi-chord b , respectively. The main modification to the original theory consists of replacing the 3-D Green’s function with a 2-D Green’s function to account for radiation in two dimensions only. Inserting the two-dimensional Green’s function into Goldstein’s formulation⁵ of the acoustic analogy (neglecting viscosity and performing a Fourier transform in time) yields

$$p(\underline{x}, \omega) = \frac{\mathbf{i}x_2\omega b}{4\beta c} \int_{-2}^0 \Delta p_t(\underline{y}, \omega) \frac{1}{R} H_1^{(2)} \{ \mu_0 [M(y_1 - x_1) + R] \} dy_1 . \quad (1)$$

where ω is the frequency, $\beta = \sqrt{1 - M^2}$, $R = \sqrt{(y_1 - x_1)^2 + \beta^2(y_2 - x_2)^2}$, and c represents the speed of sound. The reduced frequency is $\mu_0 = \omega b / (c\beta^2)$ and $H_1^{(2)}$ denotes a first-order Hankel function of the second kind. Note that, in contrast to the original theory, no far field approximation has been made.

From DNS the entire time-series of the total pressure difference Δp_t is available, and (1) can be integrated directly to obtain the acoustic pressure field. In cases where only

the incident pressure field is known, the total pressure field at the trailing edge can be determined from the incident pressure field through a transfer function⁶. This surface pressure jump transfer function has been shown to perform very well for different Mach numbers and reduced frequencies².

2.2 Direct Numerical Simulations

For DNS, the full compressible Navier–Stokes equations need to be solved. The fluid is assumed to be an ideal gas with constant specific heat coefficients. Nondimensionalizing all variables using the flow-quantities at the freestream/inflow location, the non-dimensional continuity, momentum and the energy equations are:

$$\frac{\partial \rho}{\partial t} + \frac{\partial}{\partial x_k} (\rho u_k) = 0, \quad (2)$$

$$\frac{\partial}{\partial t} (\rho u_i) + \frac{\partial}{\partial x_k} [\rho u_i u_k + p \delta_{ik} - \tau_{ik}] = F_i, \quad (3)$$

$$\frac{\partial}{\partial t} (\rho E) + \frac{\partial}{\partial x_k} \left[\rho u_k \left(E + \frac{p}{\rho} \right) + q_k - u_i \tau_{ik} \right] = 0, \quad (4)$$

where F_i is a volume force and the total energy is defined as $E = T / [\gamma(\gamma - 1)M^2] + 0.5u_i u_i$. The stress tensor and the heat-flux vector are computed as

$$\tau_{ik} = \frac{\mu}{Re} \left(\frac{\partial u_i}{\partial x_k} + \frac{\partial u_k}{\partial x_i} - \frac{2}{3} \frac{\partial u_j}{\partial x_j} \delta_{ik} \right), \quad q_k = \frac{-\mu}{(\gamma - 1)M^2 Pr Re} \frac{\partial T}{\partial x_k}, \quad (5)$$

respectively, where the Prandtl number is assumed to be constant at $Pr = 0.72$, and $\gamma = 1.4$. The molecular viscosity μ is computed using Sutherland’s law⁷, setting the ratio of the Sutherland constant over freestream temperature to 0.36867. To close the system of equations, the pressure is obtained from the non-dimensional equation of state $p = (\rho T) / (\gamma M^2)$. In order to introduce disturbances into the boundary layers, a volume force F_i is added to the right-hand-side of the governing equations. To minimize the sound generation of the disturbances, a solenoidal and therefore quiet forcing is used⁸.

$$F_1 = \frac{\partial \phi}{\partial x_2}, \quad F_2 = -\frac{\partial \phi}{\partial x_1}, \quad \text{with} \quad (6)$$

$$\phi = A_{dist} \sin(\omega t) \cdot \left[1 - \cos \left(\frac{(x_1 - x_{1b})\pi}{x_{1e} - x_{1b}} \right) \right] \cdot \left[1 - \cos \left(\frac{(x_2 - x_{2b})\pi}{x_{2e} - x_{2b}} \right) \right], \quad (7)$$

where x_{1b} and x_{1e} are the start and end points of the forcing, respectively.

3 Numerical Method

For the analytical approach, equation (1) is integrated using a fourth-order accurate integration. To reduce the computational cost, the plate is discretized with a non-uniform grid, clustering most points in the vicinity of the trailing edge.

The compressible Navier–Stokes equations, (2)-(4), are solved using a high-order accurate numerical scheme free of upwinding, artificial dissipation or any type of explicit filtering. Stability is achieved through appropriate conditioning of the governing equations, with an entropy-splitting approach for the nonlinear terms, and a Laplacian formulation of the viscous and heat conduction terms. The latter is used to avoid odd-even decoupling when using central finite-difference schemes. In addition, compatible spatial difference operators for the interior and boundary points are employed. Further details on the fundamental numerical approach are given in Sandham *et.al.*⁹. A nonreflecting zonal boundary condition is used to avoid spurious pressure-oscillations from the boundaries, in particular the outflow boundary^{3,4}.

A thorough validation of both numerical codes was performed. The non-equidistant integration used for the theoretical approach was shown to reproduce Amiet’s closed form results, and it was demonstrated that the Navier–Stokes code is capable of accurately representing the development of hydrodynamic instabilities².

4 RESULTS

DNS of trailing edges were conducted at two Mach numbers specifying either no-slip walls or slip walls. In both cases, a computational domain with dimensions $-2 \leq x_1 \leq 1.875$ ($-2 \leq x_1 \leq 2.125$ for the slip wall case) and $-3.25 \leq x_2 \leq 3.25$ was chosen. The infinitely thin plate is located at $-2 \leq y_1 \leq 0$ and $y_2 = x_2 = 0$. For the no-slip wall case, boundary layers develop on the top and bottom side of the surface which have a displacement thickness of $\delta^* = 5.85 \times 10^{-3}$ at the TE, resulting in $Re_{\delta^*} = 1170$. The flow in the no-slip case is discretized with 2500 and 600 non-equidistantly spaced points in the x_1 - and x_2 -direction, respectively, with the finest resolution at the TE. In the slip wall case, the resolution in the streamwise direction is decreased downstream of the trailing edge because no unsteady wake forms that needs to be resolved. Therefore, only 1280 streamwise points are used. For all cases, the surface is discretized with 620 points in the streamwise direction. A zonal characteristic boundary condition is used at the outflow (for $x_1 \geq 1.45$), and a traditional sponge employing a dissipation term is used for the upper and lower freestream boundaries ($|x_2| \geq 2.5$) and the inflow boundary ($-2 \leq x_1 \leq -1.875$).

Time-dependent forcing is introduced at $x_1 = -1.8625$ and $x_2 = 0.0025$ using (6), with $A_{dist} = 8 \times 10^{-3}$. In the no-slip wall, the nondimensional forcing frequency was set to $\omega = 6.4 \cdot \pi$ for both Mach numbers because linear stability theory predicted that Tollmien–Schlichting (TS) waves would be generated that are amplified up to the TE. The amplitude of the pressure disturbances associated with the TS wave are smaller than 1% of the mean pressure values at the TE. In the slip wall case, no viscous instability is present and the frequency can be chosen freely. Because the convection velocity of disturbances is higher in the slip wall case ($c_u \approx 1$ vs. $c_u \approx 0.4$) lower forcing frequencies were selected, namely $\omega = 4 \cdot \pi$ and $\omega = 2.5 \cdot \pi$ for $M = 0.4$ and $M = 0.6$, respectively. In the no-slip case the above parameters result in the nondimensional parameters $\mu_0 = 9.57$ and $K_x = 54.34$ at $M = 0.4$, and $\mu_0 = 18.85$ and $K_x = 50.27$ at $M = 0.6$. For the slip

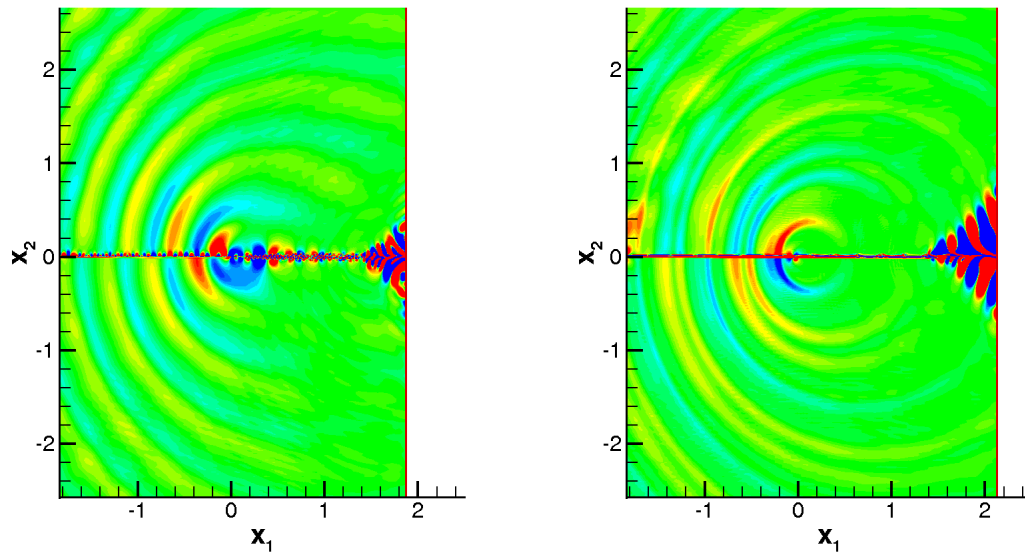


Figure 1: Contours of dilatation obtained from DNS trailing edges; no-slip wall with TS waves, $\mu_0 = 9.57$, and $K_x = 54.34$, with contour levels $[-1 \times 10^{-3}; 1 \times 10^{-3}]$ (left); slip wall, $\mu_0 = 5.98$, and $K_x = 12.57$ with contour levels $[-3 \times 10^{-5}; 3 \times 10^{-5}]$ (right); $M = 0.4$.

wall case, $\mu_0 = 5.98$ and $K_x = 12.57$, and $\mu_0 = 7.36$ and $K_x = 7.85$ at $M = 0.4$ and $M = 0.6$, respectively.

For an overview of the resulting flow fields, instantaneous contours of dilatation are shown in figures 1 and 2 for both wall boundary conditions. In the no-slip wall cases, an unsteady wake forms downstream of the TE and the TS waves on the upper side of the singular plate can clearly be seen. No wake forms in the slip-wall cases, hence only the disturbances convecting downstream are visible for $x_1 > 0$. All graphs reveal acoustic waves generated by the scattering of the disturbances at the TE. These waves radiate in both the positive and negative x_2 -directions.

In Amiet's theory⁶, it is assumed that the unsteady Kutta condition holds. Until today, there remains uncertainty regarding the accuracy of this assumption. Howe¹⁰ suggests that it might only be used for a specific frequency range and demonstrates that the imposition of the Kutta condition results in a considerable reduction of sound generated by convection of disturbances past a trailing edge. Here, DNS data are used to clarify the validity of the Kutta condition and, more importantly, to what degree the far field solution is affected by the TE boundary condition.

Figures 3 and 4 show time-series of the total pressure difference upstream of the TE and at the TE for DNS with no-slip and slip walls for $M = 0.4$ and $M = 0.6$. In the no-slip wall cases, at $y_1 = -0.1$, the total pressure differences oscillate with the forcing frequencies and an amplitude of roughly 0.01, indicating that the TS waves can be considered linear disturbances. At the trailing edge itself, the amplitudes of Δp_t are considerably decreased. However, the pressure differences do not equal zero, i.e. the unsteady Kutta condition is

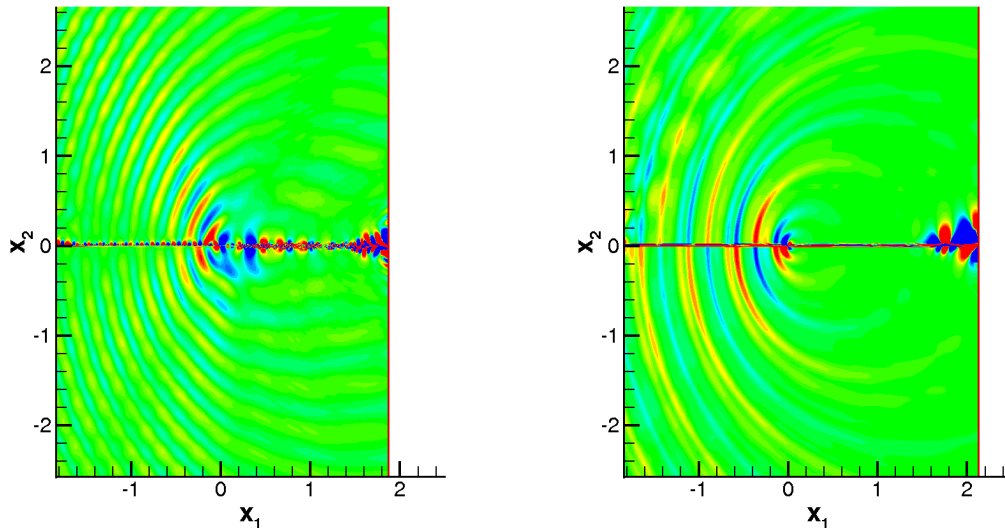


Figure 2: Contours of dilatation obtained from DNS trailing edges; no-slip wall with TS waves, $\mu_0 = 18.85$, and $K_x = 50.27$, with contour levels $[-3 \times 10^{-3}; 3 \times 10^{-3}]$ (left); slip wall, $\mu_0 = 7.36$, and $K_x = 7.85$ with contour levels $[-1 \times 10^{-4}; 1 \times 10^{-4}]$ (right); $M = 0.6$.

not satisfied for either Mach number.

In the slip wall cases, upstream of the TE, the pressure difference oscillations have a very small amplitude ($\approx 9 \times 10^{-4}$). In contrast to the viscous wall cases, the signals are not harmonic, i.e., it appears that frequencies other than the respective forcing frequencies are present. More importantly, the amplitudes of the pressure difference at the trailing edge are significantly greater than at $y_1 = -0.1$ (the amplitudes are divided by 10 for better legibility). This is in contrast to the no-slip wall case where most likely viscous effects in the boundary layer lead to the unsteady Kutta condition being ‘nearly’ satisfied. The sudden increase in total pressure difference towards the trailing edge might be regarded as a numerical issue in the calculation with a slip wall. Therefore, the DNS were repeated,

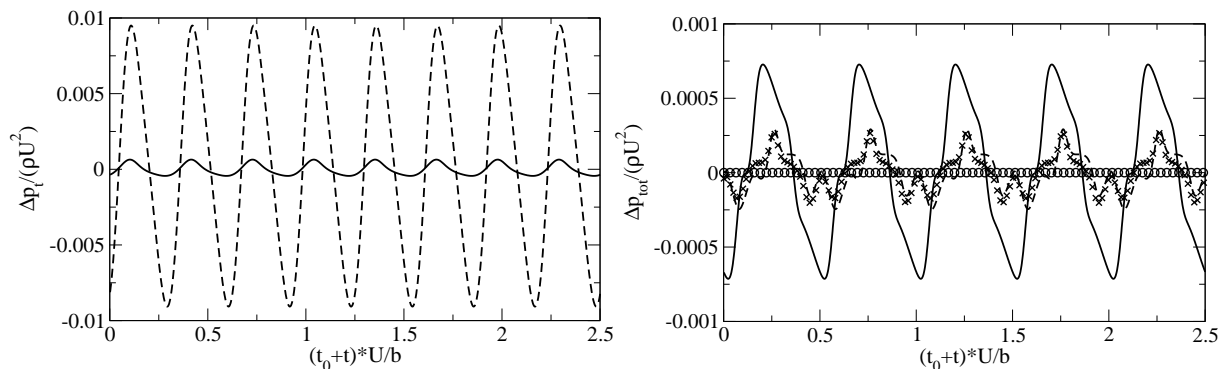


Figure 3: Total pressure difference Δp_t from DNS for no-slip wall, $\omega = 6.4 \cdot \pi$ (right), and slip wall, $\omega = 4 \cdot \pi$ (left); (- -) $y_1 = -0.1$, (—) $y_1 = 0.0$, (×) $y_1 = -0.1$ with Kutta condition imposed (slip wall only), (o) at $y_1 = 0.0$ with Kutta condition imposed (slip wall only); $M = 0.4$.

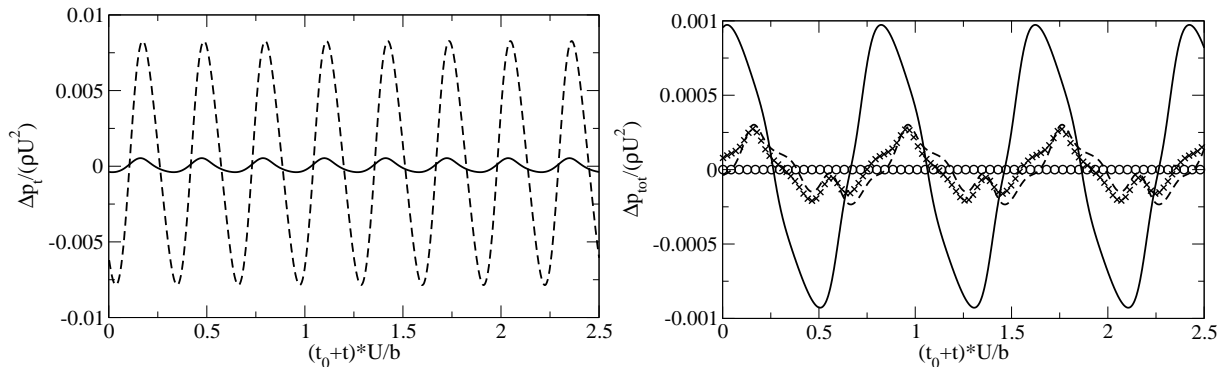


Figure 4: Total pressure difference Δp_t from DNS for no-slip wall, $\omega = 6.4 \cdot \pi$ (right), and slip wall, $\omega = 2.5 \cdot \pi$ (left); (---) $y_1 = -0.1$, (—) $y_1 = 0.0$ (divided by 10), (\times) $y_1 = -0.1$ with Kutta condition imposed (slip wall only), (\circ) $y_1 = 0.0$ with Kutta condition imposed (slip wall only); $M = 0.6$.

this time enforcing the unsteady Kutta condition at the trailing edge. From figures 3 and 4 it can be observed that imposing the unsteady Kutta condition does not considerably alter the flow just upstream of the TE, i.e. the pressure difference oscillations at $y_1 = -0.1$ are similar to those without Kutta condition.

The fact that the slip wall cases, in which the Kutta condition is not imposed, show large amplitude oscillations can be used to quantify the importance of the Kutta condition. In the following, results obtained from slip wall simulations with and without imposing the unsteady Kutta condition are examined. When specifying no-slip walls the pressure oscillations were harmonic, thus only the disturbance pressure associated with the forcing frequency needs to be analyzed. However, in the slip wall cases, multiple modes appear to be present. Therefore, in figure 5, the streamwise disturbance-pressure distribution on the top surface is illustrated for the forcing mode and the first higher harmonic. For both Mach numbers the mode associated with the forcing frequency is smaller in amplitude

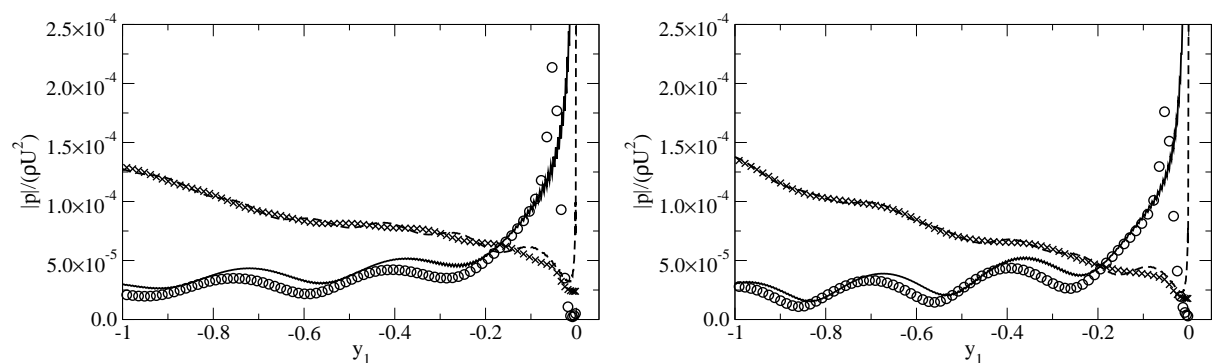


Figure 5: Magnitude of total disturbance pressure on top surface from DNS with slip walls at $M = 0.4$ and $\omega = 4 \cdot \pi$ (left), and $M = 0.6$ and $\omega = 2.5 \cdot \pi$ (right); (—) forcing frequency, (---) first higher harmonic of forcing frequency, (\circ) forcing frequency with Kutta condition imposed, (\times) first higher harmonic of forcing frequency with Kutta condition imposed.

than the first higher harmonic up to $y_1 \approx -0.175$. Approaching the TE, however, the magnitude of the fundamental mode increases dramatically and reaches an amplitude of roughly 4.6×10^{-3} when the Kutta condition is not imposed. When the unsteady Kutta condition is imposed, the pressure magnitude decreases towards the TE after reaching a maximum at $y_1 \approx -0.05$. The first higher harmonic decays up to the TE when $\Delta p_t = 0$ is enforced at the TE; however, when the pressure difference at the TE is permitted to be non-zero, a sharp increase just upstream of the trailing edge can be observed.

With the surface pressure difference available, the acoustic pressure p can now be predicted using (1) where $\Delta p_t = p_{t_{top}} - p_{t_{bottom}}$, i.e. the difference of the top and bottom surface total pressures. The results computed using 2-D theory are then compared to the acoustic pressure predicted by DNS. In DNS the acoustic pressure was obtained by conducting simulations over a period of at least four flow-through-times and computing p_{RMS} . Because of the similar magnitudes of the surface pressure of the temporal modes associated with the forcing frequency and its first higher harmonic, the acoustic pressure was computed from (1) for both modes in the slip wall cases. However, when using the mode related to the first higher harmonic, the amplitude of the acoustic pressure was more than an order of magnitude smaller than for the fundamental mode. Hence, it appears that the amplitude of the pressure distribution in the immediate vicinity of the TE is the dominant contributor to the far field noise, since the amplitude of the fundamental mode is only significantly larger than that of the higher harmonic in this region. In addition, the lower frequency is radiated more efficiently than that of the first higher harmonic.

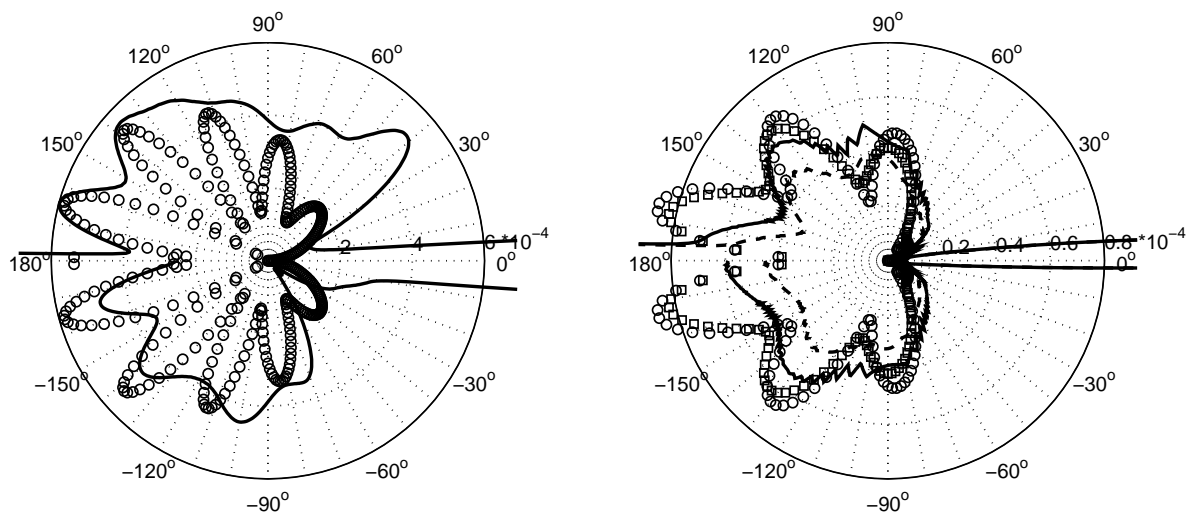


Figure 6: Magnitude of acoustic pressure at $R_d = 1.5$ for no-slip wall with $\mu_0 = 9.57$ and $K_x = 54.34$ (left), and slip wall with $\mu_0 = 5.98$ and $K_x = 12.57$ (right); (\circ) $|p|$ from (1) using $\Delta p_t = p_{t_{top}} - p_{t_{bottom}}$ from trailing edge DNS, (\square) $|p|$ from (1) using $\Delta p_t = p_{t_{top}} - p_{t_{bottom}}$ from trailing edge DNS with Kutta condition imposed (slip wall only), (—) $|p|$ from DNS, (---) $|p|$ from DNS with Kutta condition imposed (slip wall only); data from DNS multiplied by 2 and 4 for no-slip wall and slip wall, respectively; $M = 0.4$.

Results are therefore only shown for the fundamental mode.

The resulting acoustic pressure magnitudes at $R_d = 1.5$ are presented in figures 6 and 7 for both Mach numbers. To facilitate comparison the amplitudes of the DNS data in the no-slip cases were multiplied by 2 and 3 at $M = 0.4$ and $M = 0.6$, respectively, and by 4 for both Mach numbers in the slip wall cases. Most likely the lower amplitudes of the acoustic pressure obtained directly from DNS can be attributed to viscosity. This assumption is substantiated by the fact that the difference in amplitude between the (inviscid) theory and the (viscous) DNS (with no-slip walls) increases with an increase in reduced frequency. It is well known that higher frequencies are more strongly damped by viscosity. However, it is slightly surprising that the acoustic pressure obtained from DNS with slip walls needs to be scaled by an even greater factor to achieve a similar amplitude than 2-D theory. It might be due to the fact that there is no superposition of the wake noise in the slip wall cases.

When specifying no-slip walls, the agreement of the 2-D theory with the DNS data is reasonable in terms of the location of the maxima and minima, when considering the upstream inclined lobes. However, the downstream pointing lobes are much more significant in the DNS data than predicted by theory and the lobes in the DNS are smeared. The smearing of the lobes was attributed to the presence of the boundary layers and noise generated by the unsteady wake². In addition, nonlinear interaction of the TS waves with Kelvin–Helmholtz instability waves in the wake was identified as the potential origin of the pronounced downstream pointing lobes in the no-slip wall cases. The absence of the

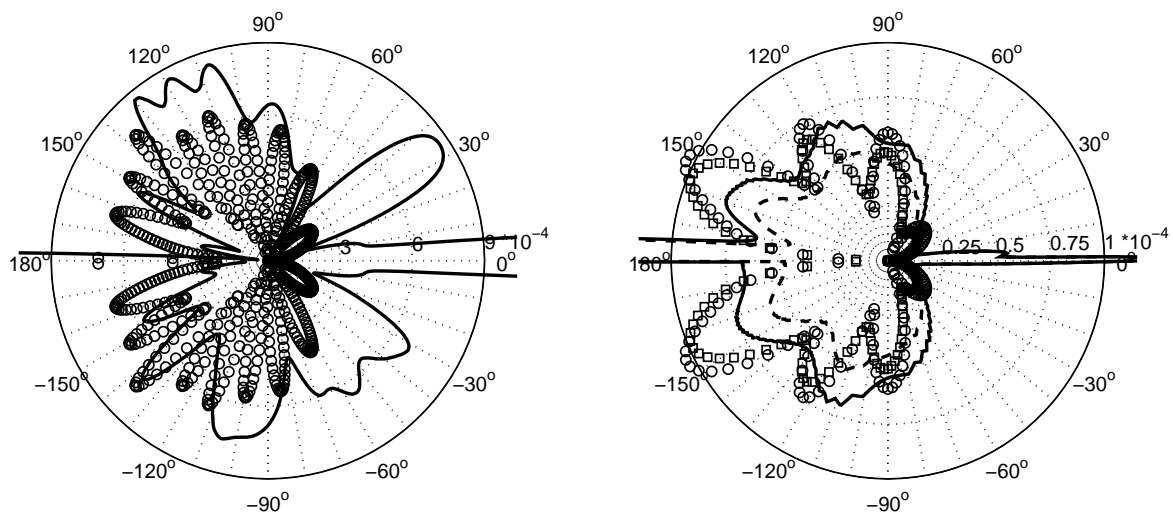


Figure 7: Magnitude of acoustic pressure at $R_d = 1.5$ for no-slip wall with $\mu_0 = 18.85$ and $K_x = 50.27$ (left), and slip wall with $\mu_0 = 7.36$ and $K_x = 7.85$ (right); (o) $|p|$ from (1) using $\Delta p_t = p_{t_{top}} - p_{t_{bottom}}$ from trailing edge DNS, (\square) $|p|$ from (1) using $\Delta p_t = p_{t_{top}} - p_{t_{bottom}}$ from trailing edge DNS with Kutta condition imposed (slip wall only), (—) $|p|$ from DNS, (---) $|p|$ from DNS with Kutta condition imposed (slip wall only); data from DNS multiplied by 2 and 4 for no-slip wall and slip wall, respectively; $M = 0.6$.

downstream-pointing lobes in the slip wall cases (which do not exhibit an unsteady wake) constitutes further evidence that these lobes might indeed be generated through interaction of the TS waves and the wake. The overall agreement between slip wall DNS data and 2-D theory is generally better than in the no-slip cases, i.e. no significant smearing of the lobes can be observed, and the acoustic pressure obtained from DNS in the slip wall cases displays a highly symmetric behavior with respect to $x_2 = 0$, as predicted by theory. This was expected as the slip wall simulations reflect the assumptions made when deriving the theory (inviscid flow, the convection speed of disturbances being close to the freestream velocity, etc.) more closely than the no-slip wall simulations.

Finally, the results of slip wall simulations with and without imposing the unsteady Kutta condition are compared. The shape of the directivity distribution is similar regardless of the trailing edge boundary condition. However, when enforcing $\Delta p_t = 0$ at the TE, the amplitude of the acoustic pressure obtained either from DNS or using 2-D theory is decreased. It was shown in figure 5 that the surface pressure distributions for cases with and without an explicit Kutta condition are similar up to $y_1 \approx -0.05$. This corroborates the above statement that the amplitude of the pressure distribution in the immediate vicinity of the TE is the dominant contributor to the far field noise. Nevertheless, despite the large fluctuations of Δp_t at the trailing edge when the Kutta condition is not specified, the difference in the amplitude of p is moderate. This implies that satisfaction of the unsteady Kutta condition at the trailing edge is not crucial for making accurate prediction of the far field noise.

5 CONCLUSIONS

Two-dimensional direct numerical simulations of infinitely thin trailing edges were conducted at $M = 0.4$ and $M = 0.6$. On the surface, either no-slip or slip wall conditions were specified. The difference in the wall boundary condition results in two distinct features of the no-slip wall case which are not present in slip wall calculations: i) the presence of boundary layers, and ii) the formation of an unsteady wake. Thus, by comparing the simulations, the effects of the boundary layers and the unsteady wake on the far field pressure can be investigated.

The DNS revealed that the unsteady Kutta condition is not satisfied, irrespective of the wall boundary condition. For slip wall simulations, the pressure difference at the trailing edge is considerably larger than in the no-slip wall cases. Additional DNS were conducted with an imposed unsteady Kutta condition in order to evaluate the far field effect of the pressure fluctuations at the trailing edge. Overall, it was found that satisfaction of the unsteady Kutta condition at the trailing edge is not essential for making accurate prediction of the far field noise. In addition, circumstantial evidence was presented showing that the surface pressure distribution in the immediate vicinity of the TE is the dominant contributor to the far field noise.

A comparison of data from no-slip and slip wall simulations provided further evidence that the downstream pointing lobes in the no-slip wall cases are due to nonlinear inter-

action of the TS waves and instability waves in the wake. Slip wall DNS data also did not display significant smearing of the lobes, confirming that this effect is most likely caused by the presence of boundary layers and noise generated by the unsteady wake in the no-slip wall simulations.

This work was supported by the DTI under the MSTTAR DARP programme. Computer time was partly provided by the EPSRC grant GR/S27474/01.

REFERENCES

- [1] R.K. Amiet. Noise due to turbulent flow past a trailing edge. *J. Sound and Vibration*, **47**(3), 387–393, (1976).
- [2] R. D. Sandberg, N. D. Sandham, and P. F. Joseph. DNS of trailing-edge noise generated by boundary-layer instabilities. *AIAA Paper 2006-2514*. 12th AIAA/CEAS Aeroacoustics Conference (27th AIAA Aeroacoustics Conference), (2006).
- [3] R. D. Sandberg and N. D. Sandham. Nonreflecting zonal characteristic boundary condition for direct numerical simulation of aerodynamic sound. *AIAA J.*, **44**(2), 402–405, (2006).
- [4] R. D. Sandberg, L. E. Jones, and N. D. Sandham. A zonal characteristic boundary condition for numerical simulations of aerodynamic sound. In P. Wesseling, E. Oñate, and J. Périaux, editors, *European Conference on Computational Fluid Dynamics, ECCOMAS CFD 2006*, (2006).
- [5] M. E. Goldstein. *Aeroacoustics*. McGraw-Hill, 1st edition, (1976).
- [6] R.K. Amiet. High-frequency thin airfoil theory for subsonic flow. *AIAA J.*, **14**(8), 1076–1082, (1976).
- [7] F. M. White. *Viscous Fluid Flow*. McGraw Hill, (1991).
- [8] M. Wei and J.B. Freund. A noise-controlled free shear flow. *J. Fluid Mech.*, **546**, 123–152, (2006).
- [9] N.D. Sandham, Q. Li, and H.C. Yee. Entropy splitting for high-order numerical simulation of compressible turbulence. *J. Comp. Phys.*, **178**, 307–322, (2002).
- [10] M. S. Howe. The influence of vortex shedding on the generation of sound by convected turbulence. *J. Fluid Mech.*, **76**(4), 711–740, (1976).